Intervalence charge transfer and charge transport in the spinel ferrite ferromagnetic semiconductor Ru-doped CoFe$_2$O$_4$

Masaki Kobayashi [1,2,*] Munetoshi Seki [1,2] Masahiro Suzuki,[3] Ryo Okano,[1] Miho Kitamura,[5] Koji Horiba,[5]
Hiroshi Kumigashira,[5,6] Atsushi Fujimori,[3,4] Masaaki Tanaka,[1,2] and Hitoshi Tabata[1,2]

[1]*Department of Electrical Engineering and Information Systems, The University of Tokyo, 7-3-1 Hongo, Bunkyo-ku, Tokyo 113-8656, Japan*
[2]*Center for Spintronics Research Network, The University of Tokyo, 7-3-1 Hongo, Bunkyo-ku, Tokyo 113-8656, Japan*
[3]*Department of Physics, The University of Tokyo, 7-3-1 Hongo, Bunkyo-ku, Tokyo 113-0033, Japan*
[4]*Department of Applied Physics, Waseda University, Okubo, Shinjuku, Tokyo 169-8555, Japan*
[5]*Photon Factory, Institute of Materials Structure Science, High Energy Accelerator Research Organization (KEK),
1-1 Oho, Tsukuba 305-0801, Japan*
[6]*Insitute of Multidisciplinary Research for Advanced Materials (IMRAM), Tohoku University, Sendai 980-8577, Japan*

Intervalence charge transfer (IVCT) refers to the transfer of electrons between two metal (M) sites with different oxidation states, through a bridging ligand: $M^{n+1} + M'^m \rightarrow M^n + M'^{m+1}$. It is considered that the IVCT is related to the hopping probability of electrons (or electron mobility) in solids. Controlling the conductivity of ferromagnetic semiconductors (FMSs) is critical for device applications, and thus, the manipulation of conductivity through IVCT may be an approach of band engineering in FMSs. In Ru-doped CoFe$_2$O$_4$ (CFO), which shows ferrimagnetism and semiconducting transport properties, the reduction in electric resistivity is attributed to both carrier doping caused by the Ru substitution of Co and increase in carrier mobility due to hybridization between the wide Ru 4d and Fe 3d orbitals. The latter indicates the so-called IVCT mechanism, i.e., charge transfer between the mixed valence Fe^{2+}/Fe^{3+} states, facilitated by the bridging Ru 4d orbital, expressed as Fe^{2+} + Ru^{4+} ↔ Fe^{3+} + Ru^{3+}. To elucidate the emergence of the IVCT state, we conducted x-ray absorption spectroscopy (XAS) and resonant photoemission spectroscopy (RPES) measurements on undoped CFO and Ru-doped Co$_{0.5}$Ru$_{0.5}$Fe$_2$O$_4$ (CRFO) thin films. The XAS and RPES spectra indicated the presence of mixed valence Fe^{2+}/Fe^{3+} states and hybridization between the Fe 3d and Ru 4d states. These results provide experimental evidence for the IVCT state in CRFO, demonstrating a mechanism that controls electron mobility through hybridization between the 3d transition metal cations with intervening 4d states.

I. INTRODUCTION

Intervalence charge transfer (IVCT) occurring in mixed valence coordination complexes is an electron transfer process between two metal M sites differing in oxidation states through a bridging ligand $M^{n+1} + M'^m \rightarrow M^n + M'^{m+1}$ and is usually related to the photoexcitation phenomena in these compounds [1,2]. Additionally, magneto-optical properties of ferrites or iron oxides originating from IVCT, such as magneto-optical Kerr rotation and photoinduced magnetization, have been reported thus far [3–8]. In semiconducting or insulating materials with mixed valence states, especially for metal-organic frameworks, IVCT is likely related to the transport properties with hopping conduction [6,9–13]. Thus, one can control the magneto-optical and transport properties of mixed valence semiconductors or insulators through IVCT.

Ferromagnetic semiconductors (FMSs) having both semiconducting and ferromagnetic properties are key materials for spintronics, in which both the charge and spin degrees of freedom are utilized for developing functional electronic devices

[14–16]. Controlling the conductivity of FMSs while maintaining their ferromagnetic properties is useful for applying FMSs to spintronic devices, such as magnetic random-access memories and spin transistors. Spinel ferrites, represented by the chemical formula MFe$_2$O$_4$ [$M = 3d$ transition metals (TMs)], are promising for spintronics because of their chemical stability and high Curie temperatures [17]. Indeed, spinel-ferrite layers in magnetic tunnel junctions act as spin filters, as demonstrated in previous studies [18,19]. CoFe$_2$O$_4$ (CFO) with an inverse spinel structure shows ferrimagnetism with the Curie temperature (T_C) of 793 K, and CFO epitaxial thin films have been studied for application to spintronic devices [10,20–23]. In CFO, the ideal valence states of the constituent Co and Fe ions are Co^{2+} at the octahedral crystal-field (O_h) site and Fe^{3+} at both the O_h and the tetrahedral crystal-field (T_d) sites, as shown in Fig. 1. Recently, Iwamoto *et al.* [10] succeeded in increasing the conductivity of CFO via Ru doping; the Ru^{3+} or Ru^{4+} ions occupy the Co^{2+} sites preferentially in CFO [7,10]. As shown in Fig. 2, the transport properties of the Ru-doped CFO thin films demonstrate that the Ru doping increases both the carrier density and electron mobility. The doped Ru ions in Co$_{0.5}$Ru$_{0.5}$Fe$_2$O$_4$ (CRFO) are expected to act as double donors. Furthermore, the Ru doping
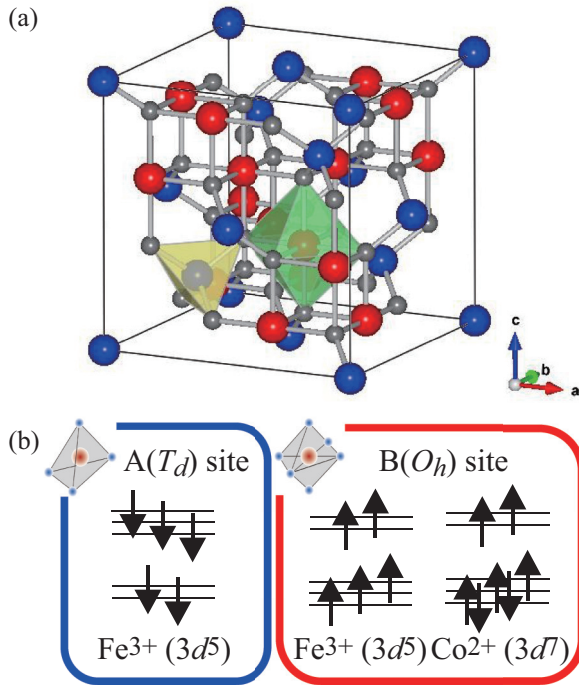
*masaki.kobayashi@ee.t.u-tokyo.ac.jp

FIG. 1. Crystal structure of the inverse spinel CFO. (a) Unit cell of CFO. The magnetic sublattice of the A(T_d) site antiferromagnetically couples with that of the B(O_h) site. (b) Spin configurations of the A and B sites.

increases the carrier concentration as well as the hopping probability though hybridization between the Fe $3d$ and Ru $4d$ orbitals. It is considered that the electron carriers supplied by the doped Ru ions generate the mixed valence state of
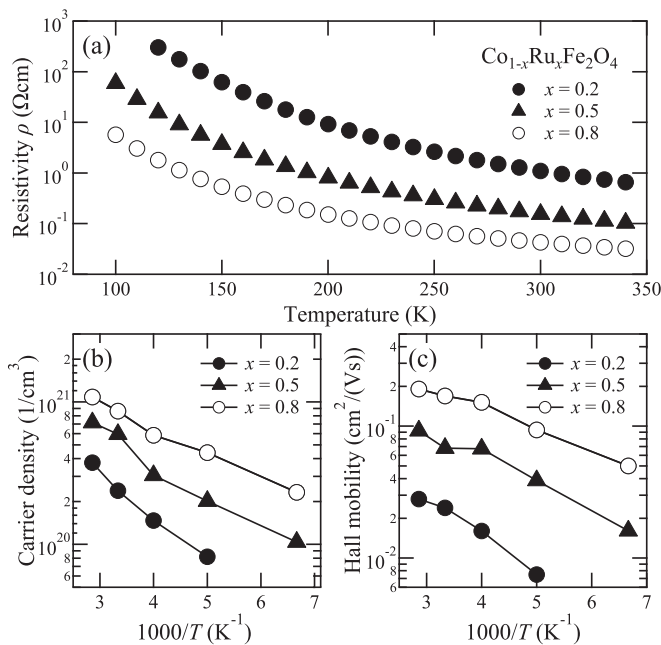

FIG. 2. Transport properties of the $Co_{1-x}Ru_xFe_2O_4$ thin films [10]. (a) Temperature (T) dependence of resistivity (ρ). (b) and (c) Compositional dependence of the carrier density and Hall mobility, respectively.

Fe^{2+}/Fe^{3+}, increasing the conductivity through carrier hopping between the Fe^{2+} and Fe^{3+} sites, like that in metallic Fe_3O_4. First-principles band structure calculation supports the idea that the increase in hopping conduction occurs through the hybridization between the Fe $3d$ and Ru $4d$ orbitals following the IVCT mechanism, i.e., $Fe^{2+} + Ru^{4+} \leftrightarrow Fe^{3+} + Ru^{3+}$ [10].

To prove the existence of such an IVCT mechanism in CRFO, two key factors should be experimentally confirmed: (1) the Fe^{2+}/Fe^{3+} mixed valence state and (2) the hybridization between the Fe $3d$ and Ru $4d$ orbitals. In this paper, we investigated undoped and Ru-doped CFO thin films using x-ray absorption spectroscopy (XAS) and resonance photoemission spectroscopy (RPES) to obtain experimental evidence for the IVCT state in CRFO. XAS and RPES enable us to probe element- and orbital-specific electronic structures. The XAS spectra revealed the valence states of Fe and Co in CRFO, whereas the RPES spectra indicated that the partial density of states (PDOS) of Fe $3d$ changed with Ru doping. These experimental findings support the successful realization of the IVCT state in Ru-doped CFO. The manipulation of conductivity through IVCT may become an approach of band engineering in FMS materials.

II. EXPERIMENTAL

The CFO and CRFO epitaxial thin films were grown on single-crystal α-Al_2O_3(0001) substrates using the pulsed laser deposition technique with an ArF excimer laser with a wavelength of 193 nm, frequency of 5 Hz, and fluence $E = 60$ mJ. The details of the thin film growth are described elsewhere [10]. The thickness of each film was $\sim$90 nm, which was larger than the critical thickness of 1.1 nm required for strain relaxation. The RPES and XAS measurements were performed at the BL-2A beamline in Photon Factory, High Energy Accelerator Research Organization (KEK) [24]. For the RPES measurements, the total energy resolution was set to 100–250 meV using a photon energy in the range of 400–1200 eV. The binding energies were calibrated by measuring the Fermi level (E_F) of a gold foil, which was electrically connected to the samples. The RPES measurements were conducted with an SES2002 electron analyzer at room temperature under a base pressure $<2.0 \times 10^{-8}$ Pa. The XAS spectra were measured in the total electron yield mode.

III. RESULTS AND DISCUSSION

A. Co $L_{2,3}$ XAS

Figure 3 shows the Co $L_{2,3}$ XAS spectra of the undoped and Ru-doped CFO (i.e., CRFO), revealing multiplet structures. A comparison of the observed Co $L_{2,3}$ spectra with those of the reference compounds CoO (Co^{2+} O_h) and $LaCoO_3$ (Co^{3+} O_h) [25] indicates that the spectrum of CRFO is like that of CoO, whereas the spectrum of CFO is a superposition of these two spectra. The presence of Co^{3+} ions in the CFO film is attributed to cation inversion or Co antisite defects (cation exchange between Fe and Co at A and B sites, respectively), i.e., we assumed that the oxidation state of the Co ions occupying the A site was Co^{3+} and that of the Fe ions moving from the A site to the B site was Fe^{3+}. Although the
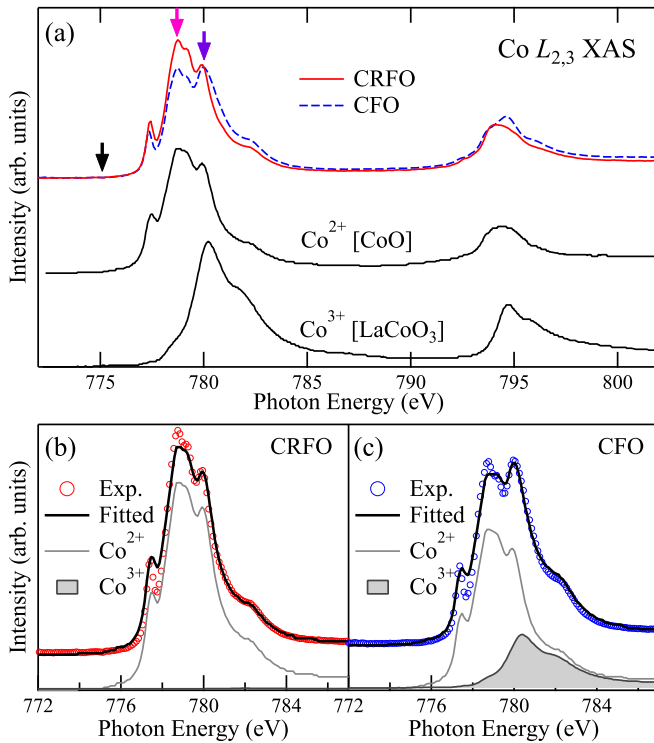
FIG. 3. Co $L_{2,3}$ x-ray absorption spectroscopy (XAS) spectra of the $Co_{1-x}Ru_xFe_2O_4$ thin films. (a) XAS spectra of the parent CFO and CRFO thin films. The spectra of CoO (Co^{2+}) and $LaCoO_3$ (Co^{3+}) are also shown as references [25]. The arrows indicate the excitation energies for resonant photoemission spectroscopy (RPES), i.e., 775 eV for off resonance, 778.7 eV for the Co^{2+} on resonance, and 780 eV for the Co^{3+} on resonance. (b) and (c) Decomposition of the Co $L_{2,3}$ spectra of the CRFO and CFO thin films, respectively.

XAS spectrum of the Co^{3+} O_h was like that of the Co^{3+} T_d [26], under the assumption that the Co ions occupying the A site become Co^{3+} and a fraction of the Fe ions at the B site become Fe^{2+} to maintain the charge neutrality. The Co and Fe $L_{2,3}$-edge XAS spectra of CFO presented in Fig. 3 can be consistently explained as described below.

To estimate the ratio of different oxidation (valence) states of Co, the Co $L_{2,3}$ XAS spectra of CFO and CRFO were fitted by a linear combination of the reference spectra of CoO and $LaCoO_3$. Figures 3(b) and 3(c) show the decomposition analyses of the Co $L_{2,3}$ XAS spectra. Figure 3(b) shows that the Co $L_{2,3}$ XAS spectrum of CRFO can be fitted by the spectrum of CoO alone, and the contribution of the Co^{3+} state to the experimental spectrum is negligible within the accuracy of the analysis. In contrast, the Co $L_{2,3}$ XAS spectrum of CFO is decomposed into Co^{2+} ($\sim 75\%$) and Co^{3+} ($\sim 25\%$) components, as shown in Fig. 3(c). This analysis suggests that a fraction of the Co^{2+} ions moved to the A site and became Co^{3+}, while a fraction of the Fe^{3+} ions at the A site moved to the B site and were converted to Fe^{2+}, maintaining the charge neutrality. This implies that the antisite defects, namely, Co ions, moved from the B site to the A site, while the Fe ions at the A site moved to the B site. This observation is consistent with the results of previous studies, in which the nonnegligible cation inversion defects were found to exist naturally in spinel
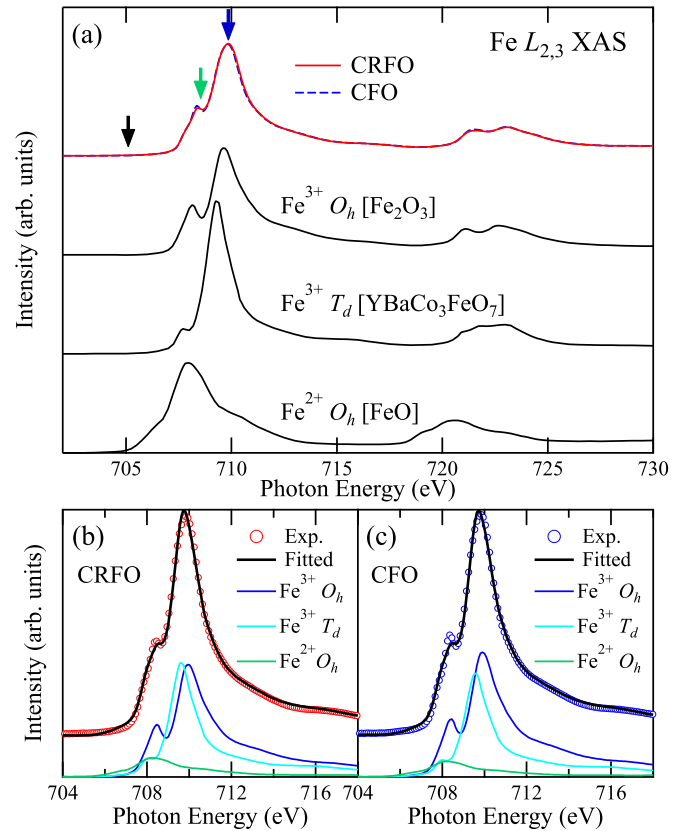

FIG. 4. Fe $L_{2,3}$ x-ray absorption spectroscopy (XAS) spectra of the $Co_{1-x}Ru_xFe_2O_4$ thin films. (a) XAS spectra of the parent CFO and CRFO thin films. The reference spectra of Fe_2O_3 (Fe^{3+} O_h) [27], $YBaCo_3FeO_7$ (Fe^{3+} T_d) [28], and FeO (Fe^{2+} O_h) [29] are also shown. The arrows represent the excitation energies for resonant photoemission spectroscopy (RPES), i.e., 705 eV for off resonance, 708.5 eV for the Fe^{2+} on resonance, and 710 eV for the Fe^{3+} on resonance. (b) and (c) Decomposition of the Fe $L_{2,3}$ spectra of the CRFO and CFO thin films, respectively.

ferrite thin films [22,23]. In contrast, in CRFO, the preferential occupation of the Ru ions at the B site [7,10,27] as well as the electron-rich environment induced by the Ru doping may suppress the formation of Co^{3+} ions and, possibly, the cation inversion as well.

B. Fe $L_{2,3}$ XAS

Figure 4 presents the Fe $L_{2,3}$ XAS spectra of the parent CFO and CRFO thin films, showing multiplet structures. Furthermore, the spectral lineshapes are like that of Fe_2O_3, as shown in Fig. 4(a). In contrast to the Co $L_{2,3}$ XAS spectra, the Fe XAS spectrum of the CRFO film appears identical to that of the CFO film. To evaluate the relative amounts of the Fe components precisely, the Fe $L_{2,3}$ XAS spectra were decomposed into various valence and crystal-field states using linear combinations of the reference spectra of Fe_2O_3 (Fe^{3+} O_h) [28], $YBaCo_3FeO_7$ (Fe^{3+} T_d) [29], and FeO (Fe^{2+} O_h) [30]. As shown in Figs. 4(b) and 4(c), the linear combinations of the reference spectra well-reproduced the observed spectra of the CRFO and CFO samples. The ratios of the components are listed in Table I. As expected from the lineshapes, the ratio of

TABLE I. Decomposition analysis for the Co $L_{2,3}$ and Fe $L_{2,3}$ XAS spectra. The Co^{2+} components include both the Co^{2+} ions at the B site and the possible antisite defects of Co^{2+} at the A site.

	A(T_d) site		B(O_h) site		
	Co^{3+}	Fe^{3+}	Co^{2+}	Fe^{3+}	Fe^{2+}
$CoFe_2O_4$	25%	33.6%	75%	57.9%	8.5%
$Co_{0.5}Ru_{0.5}Fe_2O_4$	0%	37.2%	100%	52.3%	10.5%

the Fe components in the CRFO film is like that in the CFO film.

The existence of the cation-inversion defects in the CFO thin film, as observed in the Co $L_{2,3}$ XAS spectrum, indicates that Fe^{2+} in the CFO film likely originates from the Fe antisite defect, where the excess Fe ions at the B site substitute the Co^{2+} ions and become Fe^{2+}. Based on the analysis, the chemical composition of CFO is estimated as

$$[Co^{2+} O_h]^B_{0.75}[Co^{3+} T_d]^A_{0.25}[Fe^{3+} T_d]^A_{0.70}$$
$$\times [Fe^{3+} O_h]^B_{1.15}[Fe^{2+} O_h]^B_{0.15}.$$

This analyzed composition is consistent with the ratio between the T_d and O_h sites (1:2) and fulfills the charge neutrality, suggesting that the Co^{3+} ions are likely substituted in the A site.

In contrast, the Fe^{2+} ions in the CRFO film were possibly induced by electron doping caused by the Ru substitution because there were only a few cation-inversion defects in the CRFO film. Although the ratio of Fe^{2+} was expected to be 37.5% of the Fe ions in CRFO, based on the nominal composition $Co_{0.5}Ru_{0.5}Fe_2O_4$ and the assumption that the doped Ru ions substituting Co^{2+} donate electrons to the Fe^{3+} ions, the observed Fe^{2+} ratio was extremely small ($\sim$10.5%). Because CRFO contained a negligible amount of Co^{3+} ions, this quantitative discrepancy may have originated from the Ru antisite defects substituting the Fe sites. Assuming the mixed valence state of the Ru ions with the ratio of m [31], the chemical composition of CRFO is expected as

$$[Co^{2+} O_h]^B_{0.5}[Ru^{4+} T_d]^A_m[Ru^{3+} O_h]^B_{0.5-m}[Fe^{3+} T_d]^A_{0.75}$$
$$\times [Fe^{3+} O_h]^B_{1.05}[Fe^{2+} O_h]^B_{0.2},$$

where the value of m is estimated as $\sim$0.2 because of the ratio between the T_d and O_h sites. The average valency of the cation sites is $\sim$2.85, which is reasonable for the chemical composition of CRFO. Thus, these results provide spectroscopic evidence for the Ru-doping-induced Fe^{2+}/Fe^{3+} mixed valence state in the CRFO thin film. However, antisite defects must be assumed to explain the observed Fe^{2+}/Fe^{3+} ratio quantitatively.

C. 3d PDOS in the valence band

Hybridization is another key factor leading to IVCT. To elucidate the hybridization between the Fe 3d and Ru 4d orbitals, the Fe and Co 3d PDOS in the valence band (VB) were obtained using RPES. Figure 5 shows the RPES spectra of the CFO and CRFO thin films. When the incident photon with an energy of $h\nu$ leads to core-hole excitation, photoemission
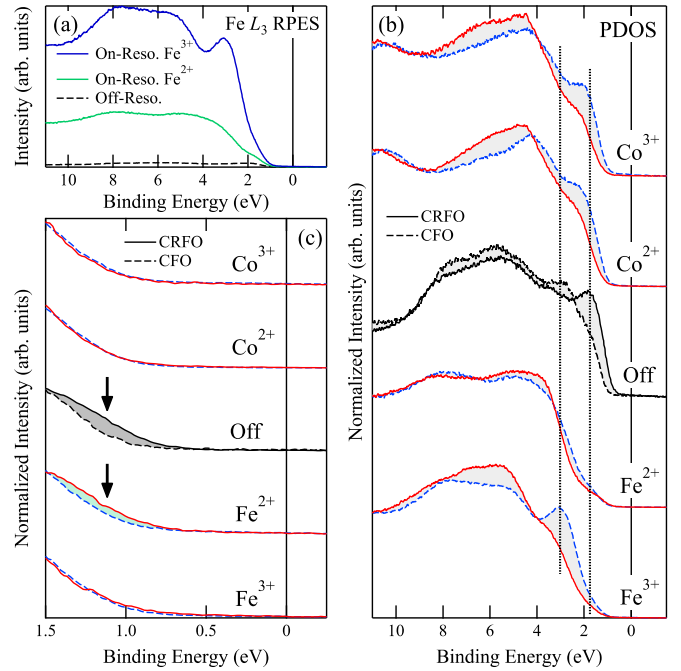

FIG. 5. Resonant photoemission spectra of the Fe L_3 and Co L_3 edges of the $Co_{1-x}Ru_xFe_2O_4$ thin films. (a) On- and off-resonance Fe L_3 edge spectra of CFO. (b) Partial density of states (PDOS) of the Fe 3d and Co 3d states. The shaded areas indicate the difference between the PDOS of the CFO and CRFO films. The spectra are normalized to the intensity integrated from E_F to $E_B \sim 11$ eV. (c) Fe 3d and Co 3d PDOS near the valence band maximum (VBM). The spectra are normalized to the intensity at $E_B = 1.5$ eV to emphasize the spectral change near the VBM.

intensity from the valence orbital involved in the core-hole excitation is resonantly enhanced. The difference between the on- and off-resonance spectra at the $L_{2,3}$ edge reflects the 3d PDOS of the same atom. Because the 2p-3d excitation energy for each component is different, one can obtain the PDOS dominated by each component by tuning $h\nu$ to each excitation energy (it is difficult to separate these PDOS perfectly because of the overlap between the excitation peaks of the different components in the XAS spectra). For instance, as shown in Fig. 5(a), the Fe^{2+} and Fe^{3+} PDOS of the thin films were obtained from the on-resonance spectra measured at an $h\nu$ of 708.5 and 710 eV, respectively. Figure 5(b) shows the Fe and Co 3d PDOS and the off-resonance spectra of the CFO and CRFO films. Here, the on-resonance spectra were recorded at the core-hole excitation energies for the Co^{2+}, Co^{3+}, Fe^{2+}, and Fe^{3+} states and were normalized to the spectral area. For the Co 3d PDOS, the differences between the spectra of the two samples reflect the effect of Ru substitution at the Co sites. Because the Co 3d spectral intensity near the VB maximum (VBM) decreases with Ru doping, the Co 3d PDOS exhibits a negligible contribution to the conductivity increase. Similarly, the Fe^{3+} PDOS shows nearly the same spectral changes as those of Co 3d with Ru doping, suggesting negligible contributions of the Fe^{3+} ions to the increase in conductivity.

Notably, the differences between the Co off-resonance spectra of the CFO and CRFO films reflect the Ru 4d PDOS and the decrease in the Co 3d PDOS with Ru doping. The

photoemission cross-section of the atomic orbitals indicate that the VB spectra without resonance mainly reflect the Ru $4d$ PDOS [32]. Because the spectral intensity near the VBM increases with Ru doping, the Ru $4d$ PDOS predominantly contributes to the DOS near the VBM. This result is qualitatively consistent with the increase in conductivity with Ru doping. To reveal the Co and Fe $3d$ components that underwent hybridization with the Ru $4d$ orbitals, the additional Ru-doping-induced Co and Fe $3d$ PDOS near the VBM were examined. Figure 5(c) compares the various PDOS of the CFO and CFRO thin films in the vicinity of the VBM, normalized to the intensity at binding energy (E_B) ~ 1.5 eV. The comparison of the off-resonance spectra indicates that the Ru $4d$ PDOS is located near the VBM. Moreover, additional Fe^{2+} PDOS near the VBM appears with Ru doping, and the position of the Fe^{2+} PDOS is nearly the same as that of the Ru $4d$ PDOS [see the arrows in Fig. 5(c)]. In contrast, the Co^{3+}, Co^{2+}, and Fe^{3+} PDOS near the VBM exhibit the same spectral lineshapes, irrespective of the Ru doping. These observations are consistent with the first-principles calculations, which reveal that the B-site Fe $3d$ orbitals undergo hybridization with the Ru $4d$ orbitals. However, the opening of the conductivity gap in the experiment was not reproduced by the calculation [10]. The bandgap may originate from Coulomb interactions, which were not included in the calculation, i.e., a Mott gap. Thus, the present results indicate hybridization between the Fe^{2+} $3d$ and Ru $4d$ orbitals at the B site in CRFO.

D. Discussion: IVCT in FMSs

The experimental findings, i.e., the mixed valence state of Fe^{2+}/Fe^{3+} and the hybridization between the Fe $3d$ and Ru $4d$ orbitals, provide spectroscopic evidence for the IVCT state in Ru-doped CFO, namely, CRFO. In CRFO, the O $2p$ orbitals of the nearest neighbor atoms of the B sites directly bonded with the Fe $3d$ e_g and Ru $4d$ e_g orbitals at the B site. It is likely that the O $2p$ orbitals of the ligand bridge the electron hopping between the Fe and Ru atoms through $Fe^{2+} + Ru^{4+} \leftrightarrow Fe^{3+} + Ru^{3+}$. In general, the IVCT for photoexcitation is expressed with a single-headed arrow between the M atoms; here, we used a double-headed arrow to represent the IVCT for transport. In contrast to the M-M' distances that are in the range of 10–25 Å in coordination complexes, wherein IVCT has been reported [2], the effective distance for IVCT may increase in single-crystalline TM compounds like spinel ferrite oxides because the ligand bands bridging the IVCT are extended in the entire crystal. Compared with the M-M' distance in coordination complexes, in which photoexcitation induces charge transfer in a highly insulating environment, the longer effective distances for IVCT in TM compounds result in an increased hopping probability (or electron mobility) due to IVCT as well as a reduced energy barrier for the charge transfer. This may explain the increase in conductivity of Fe_2O_3 by Rh doping ($Fe_{1.8}Rh_{0.2}O_3$) [33]; in this case, the doped Rh^{3+} ions are isovalently substituted

at the Fe^{3+} sites. The same mechanism may also explain the increase in hopping probability through IVCT in $FeTiO_3$ ilmenite [9], i.e., $Fe^{2+} + Ti^{4+} \leftrightarrow Fe^{3+} + Ti^{3+}$. In Fe_3O_4 and $(La, Sr)MnO_3$, the double-exchange interaction between the magnetic ions with mixed valence states stabilizes the ferromagnetic behavior and increases the metallic conductivity [34]. In contrast, the conduction mechanism through IVCT in solids is applicable for FMS materials having low carrier concentrations with hopping conduction. Furthermore, as described in the Introduction section, the IVCT may modify the optical properties of semiconducting materials as well as the magneto-optical properties of ferrites or iron oxides [3–8]. The aforementioned analysis suggests that controlling the IVCT in FMSs with mixed valence states is an approach for manipulating the electron mobility and magneto-optical properties through hybridization between the TM d orbitals while maintaining the ferromagnetic behavior.

IV. CONCLUSIONS

In this paper, we investigated the electronic structure of Ru-doped CFO using XAS and RPES to demonstrate the emergence of IVCT in semiconducting materials. The Co $L_{2,3}$ XAS spectra indicated that, although 25% of the Co atoms exist as Co^{3+} in the CFO thin film, all the Co atoms exist as Co^{2+} ions in the Ru-doped CFO thin film. The result demonstrating absence of Co^{3+} ions in the Ru-doped CFO thin film paves the way to control the defect states during the growth of spinel ferrites. The Fe $L_{2,3}$ XAS spectra indicated that the Fe^{2+}/Fe^{3+} mixed valence state can be realized in both CFO and CRFO. The RPES observations demonstrated that the Ru $4d$ PDOS appears near the VBM and undergoes hybridization with the Fe^{2+} $3d$ state at the A site, not with Fe^{3+} and Co. These findings provide spectroscopic evidence for the IVCT state between the Ru $4d$ and Fe $3d$ orbitals. Controlling the IVCT through hybridization will open a way to manipulate both the magneto-optical properties and carrier mobility of FMSs.

[1] B. S. Brunschwig and N. Sutin, Coords. Chem. Rev. **187**, 233 (1999).

[2] J.-P. Launay, Chem. Soc. Rev. **30**, 386 (2001).

[3] W. F. J. Fontijn, P. J. van der Zaag, M. A. C. Devillers, V. A. M. Brabers, and R. Metselaar, Phys. Rev. B **56**, 5432 (1997).

[4] Y. Muraoka, H. Tabata, and T. Kawai, J. Appl. Phys. **88**, 7223 (2000).

[5] B. Zhou, Y.-W. Zhang, Y.-J. Yu, C.-S. Liao, C.-H. Yan, L.-Y. Chen, and S.-Y. Wang, Phys. Rev. B **68**, 024426 (2003).

[6] M. Seki, A. K. M. A. Hossain, T. Kawai, and H. Tabata, J. Appl. Phys. **97**, 083541 (2005).

[7] T. Kanki, Y. Hotta, N. Asakawa, M. Seki, H. Tabata, and T. Kawai, Appl. Phys. Lett. **92**, 182505 (2008).

[8] M. Seki, in *Iron Ores and Iron Oxide Materials*, edited by V. Sharokha (IntechOpen, London, 2018), Chap. 13.

[9] B. Zhang, T. Katsura, A. Shatskiy, T. Matsuzaki, and X. Wu, Phys. Rev. B **73**, 134104 (2006).

[10] F. Iwamoto, M. Seki, and H. Tabata, J. Appl. Phys. **112**, 103901 (2012).

[11] L. E. Darago, M. L. Aubrey, C. J. Yu, M. I. Gonzalez, and J. R. Long, J. Am. Chem. Soc. **137**, 15703 (2015).

[12] C. Hua, P. W. Doheny, B. Ding, B. Chan, M. Yu, C. J. Kepert, and D. M. D'Alessandro, J. Am. Chem. Soc. **140**, 6622 (2018).

[13] L. S. Xie, L. Sun, R. Wan, S. S. Park, J. A. DeGayner, C. H. Hendon, and M. Dincă, J. Am. Chem. Soc. **140**, 7411 (2018).

[14] H. Ohno, Science **281**, 951 (1998).

[15] S. A. Wolf, D. D. Awschalom, R. A. Buhrman, J. M. Daughton, S. von Molnár, M. L. Roukes, A. Y. Chtchelkanova, and D. M. Treger, Science **294**, 1488 (2001).

[16] I. Zutic, J. Fabian, and S. Das Sarma, Rev. Mod. Phys. **76**, 323 (2004).

[17] M. Sugimoto, J. Am. Ceram. Soc. **82**, 269 (1999).

[18] U. Lüders, A. Barthélémy, M. Bibes, K. Bouzehouane, S. Fusil, E. Jacquet, J.-P. Contour, J.-F. Bobo, J. Fontcberta, and A. Fert, Adv. Mater. **18**, 1733 (2006).

[19] K. Inomata, N. Ikeda, N. Tezuka, R. Goto, S. Sugimoto, M. Wojcik, and E. Jedryka, Sci. Technol. Adv. Mater. **9**, 014101 (2008).

[20] Y. Suzuki, R. B. van Dover, E. M. Gyorgy, J. M. Phillips, V. Korenivski, D. J. Werder, C. H. Chen, R. J. Cava, J. J. Krajewski, W. F. Peck, Jr., and K. B. Do, Appl. Phys. Lett. **68**, 714 (1996).

[21] Y. Suzuki, Annu. Rev. Mater. Res. **31**, 265 (2001).

[22] Y. K. Wakabayashi, Y. Nonaka, Y. Takeda, S. Sakamoto, K. Ikeda, Z. Chi, G. Shibata, A. Tanaka, Y. Saitoh, H. Yamagami, M. Tanaka, A. Fujimori, and R. Nakane, Phys. Rev. B **96**, 104410 (2017).

[23] Y. K. Wakabayashi, Y. Nonaka, Y. Takeda, S. Sakamoto, K. Ikeda, Z. Chi, G. Shibata, A. Tanaka, Y. Saitoh, H. Yamagami, M. Tanaka, A. Fujimori, and R. Nakane, Phys. Rev. Materials **2**, 104416 (2018).

[24] K. Horiba, H. Ohguchi, H. Kumigashira, M. Oshima, K. Ono, N. Nakagawa, M. Lippmaa, M. Kawasaki, and H. Koinuma, Rev. Sci. Instrum. **74**, 3406 (2003).

[25] J. -H. Park, S.-W. Cheong, and C. T. Chen, Phys. Rev. B **55**, 11072 (1997).

[26] S. Ya. Istomin, O. A. Tyablikov, S. M. Kazakov, E. V. Antipov, A. I. Kurbakov, A. A. Tsirlin, N. Hollmann, Y. Y. Chin, H. J. Lin, C. T. Chen, A. Tanaka, L. H. Tjeng, and Z. Hu, Dalton Trans. **44**, 10708 (2015).

[27] B. Krutzsch and S. Kemmler-Sack, Mater. Res. Bull. **19**, 1659 (1984).

[28] N. Hollmann, Z. Hu, M. Valldor, A. Maignan, A. Tanaka, H. H. Hsieh, H. -J. Lin, C. T. Chen, and L. H. Tjeng, Phys. Rev. B **80**, 085111 (2009).

[29] J. H. Park, Ph.D. thesis, University of Michigan, 1994.

[30] C. F. Chang, Z. Hu, S. Klein, X. H. Liu, R. Sutarto, A. Tanaka, J. C. Cezar, N. B. Brookes, H.-J. Lin, H. H. Hsieh, C. T. Chen, A. D. Rata, and L. H. Tjeng, Phys. Rev. X **6**, 041011 (2016).

[31] If the doped Ru ions were tetravalent, the chemical composition would be $[Co^{2+} O_h]^B_{0.5}$ $[Ru^{4+} T_d]^A_m$ $[Ru^{4+} O_h]^B_{0.5-m}$ $[Fe^{3+} T_d]^A_{0.75}$ $[Fe^{3+} O_h]^B_{1.05}$ $[Fe^{2+} O_h]^B_{0.2}$. Here, $m = 0.25$ makes the ratio between the T_d and O_h sites 1:2, while the average valence of the cation sites becomes ~ 2.93, which is too high for a spinel oxide. Thus, the average valence of the Ru ions in CRFO would be <4+.

[32] K. Horiba, H. Kawanaka, Y. Aiura, T. Saitoh, C. Satoh, Y. Kikuchi, M. Yokoyama, Y. Nishihara, R. Eguchi, Y. Senba, H. Ohashi, Y. Kitajima, and S. Shin, Phys. Rev. B **81**, 245127 (2010).

[33] M. Seki, H. Yamahara, and H. Tabata, Appl. Phys. Express **5**, 115801 (2012).

[34] C. Zener, Phys. Rev. **82**, 403 (1951).